doi:10.1093/brain/awp256 Brain 2010: 133; 406–420 | 406

BRAIN
A JOURNAL OF NEUROLOGY

Ectopic expression of polysialylated neural cell adhesion molecule in adult macaque Schwann cells promotes their migration and remyelination potential in the central nervous system

C. Bachelin,[1,2,3,*] V. Zujovic,[1,2,3,*] D. Buchet,[1,2,3] J. Mallet[1,2,3] and A. Baron-Van Evercooren[1,2,3,4]

1 Centre de Recherche de l'Institut du Cerveau et de la Moelle Epinière, Université Pierre et Marie Curie-Paris 6, UMR-S975, Paris, France
2 INSERM, UMR-975, CHU Pitié-Salpêtrière, 105 boulevard de l'Hôpital, 75634 Paris cedex 13, France
3 CNRS, UMR 7225, Paris, France
4 AP-HP, Hôpital Pitié-Salpétrière, Fédération de Neurologie, Paris, France

*These authors contributed equally to this work.

Correspondence to: A. Baron-Van Evercooren,
INSERM UMR-975, CHU Pitié-Salpêtrière,
105 boulevard de l'Hôpital,
75634 Paris cedex 13,
France
E-mail: anne.baron@upmc.fr

Recent findings suggested that inducing neural cell adhesion molecule polysialylation in rodents is a promising strategy for promoting tissue repair in the injured central nervous system. Since autologous grafting of Schwann cells is one potential strategy to promote central nervous system remyelination, it is essential to show that such a strategy can be translated to adult primate Schwann cells and is of interest for myelin diseases. Adult macaque Schwann cells were transduced with a lentiviral vector encoding sialyltransferase, an enzyme responsible for neural cell adhesion molecule polysialylation. *In vitro*, we found that ectopic expression of polysialylate promoted adult macaque Schwann cell migration and improved their integration among astrocytes *in vitro* without modifying their antigenic properties as either non-myelinating or pro-myelinating. In addition, forced expression of polysialylate in adult macaque Schwann cells decreased their adhesion with sister cells. To investigate the ability of adult macaque Schwann cells to integrate and migrate *in vivo*, focally induced demyelination was targeted to the spinal cord dorsal funiculus of nude mice, and both control and sialyltransferase expressing Schwann cells overexpressing green fluorescein protein were grafted remotely from the lesion site. Analysis of the spatio-temporal distribution of the grafted Schwann cells performed *in toto* and *in situ*, showed that in both groups, Schwann cells migrated towards the lesion site. However, migration of sialyltransferase expressing Schwann cells was more efficient than that of control Schwann cells, leading to their accelerated recruitment by the lesion. Moreover, ectopic expression of polysialylated neural cell adhesion molecule promoted adult macaque Schwann cell interaction with reactive astrocytes when exiting the graft, and their 'chain-like' migration along the dorsal midline. The accelerated migration of sialyltransferase expressing Schwann cells to the lesion site enhanced their ability to compete for myelin repair with endogenous cells, while control Schwann cells were unable to do so. Finally, remyelination by the exogenous sialyltransferase expressing Schwann cells restored the normal distribution of paranodal and nodal elements on

Received March 19, 2009. Revised August 13, 2009. Accepted September 2, 2009. Advance Access publication October 20, 2009

the host axons. These greater performances of sialyltransferase expressing Schwann cell correlated with their sustained expression of polysialylated neural cell adhesion molecule at early times when migrating from the graft to the lesion, and its progressive downregulation at later times during remyelination. These results underline the potential therapeutic benefit to genetically modify Schwann cells to overcome their poor migration capacity and promote their repair potential in demyelinating disorders of the central nervous system.

Keywords: Schwann cells; STX; migration; remyelination; CNS

Abbreviations: CNS = central nervous system; Ct-SC = control Schwann cells; d.p.t. = days post-transplantation; GFAP = glial fibrillary acidic protein; GFP = green fluorescein protein; LPC = lyso-phosphatidylcholine; MOG = myelin oligodendrocyte glycoprotein; P0 = myelin protein zero; PPSA-NCAM = polysialylated neural cell adhesion molecule; STX = sialyltransferase X; STX-SC = sialyltransferase expressing Schwann cell

Introduction

Schwann cells are potential candidates for autologous grafting in the lesioned central nervous system (CNS) (Zujovic *et al*., 2007). They constitute an accessible source of cells and are not a target of the immune system in multiple sclerosis. They remyelinate axons after transplantation in the demyelinated rodent CNS (Blakemore, 1977; Duncan *et al*., 1981; Baron-Van Evercooren *et al*., 1997; Franklin, 2002) and their newly formed myelin leads to electrophysiological and behavioural recovery (Honmou *et al*., 1996; Girard *et al*., 2005). In addition, grafted Schwann cells sustain neuronal survival and promote axonal regeneration after transplantation in models of spinal trauma (Takami *et al*., 2002; Pearse *et al*., 2004; Fouad *et al*., 2005). The use of recombinant forms of human heregulins, potent mitogens for Schwann cells, has made it possible to expand rodent, primate and human Schwann cells from limited amounts of tissue (Levi *et al*., 1995; Rutkowski *et al*., 1995; Avellana-Adalid *et al*., 1998) without impairing their ability to remyelinate and regulate electrical conductance after CNS engraftment (Imaizumi *et al*., 2000; Kohama *et al*., 2001). Furthermore, autologous transplantation of mitogen-expanded Schwann cells into the macaque demyelinated spinal cord results in repair of large areas of demyelination, with up to 55% of the axons remyelinated by the grafted cells (Bachelin *et al*., 2005). When transplanted into the demyelinated mouse spinal cord, these cells promote functional recovery that is enhanced by over expression of neurotrophins (Girard *et al*., 2005).

These compelling data raised hopes for the use of autologous Schwann cell transplantation as a potential therapeutic approach for myelin diseases. However, a major limitation has hindered the development of such an approach. Despite their high motility *in vitro*, or in the injured peripheral nerve, Schwann cells migrate poorly when grafted into the demyelinated or injured CNS. This restriction probably results from their poor interface with astrocytes (Franklin and Blakemore, 1993; Lakatos *et al*., 2003) and/or exclusion from white matter areas (Baron-Van Evercooren *et al*., 1996). Overcoming this limitation is a prerequisite when considering the necessity for remyelinating extensive and/or dispersed lesions, such as those found in multiple sclerosis patients. Thus, strategies aiming at enhancing Schwann cell migration in the adult CNS should overcome these inhibitions in order to improve the therapeutic properties of these cells in the demyelinated CNS.

The role of polysialylate (PSA) in the regulation of precursor cell migration was demonstrated during CNS development (Glaser *et al*., 2007). Its expression is upregulated in the developing CNS and downregulated post-natally, while persisting in the adult brain areas that show plasticity (Durbec and Cremer, 2001; Rutishauser, 2008). Polysialylated neural cell adhesion molecule (PSA-NCAM) positive precursors migrate more efficiently than PSA-NCAM negative neural precursors *in vitro* (Decker *et al*., 2000) and when transplanted in the developing CNS (Vitry *et al*., 2003). PSA is re-expressed by oligodendrocyte precursors during their recruitment to demyelinated lesions (Oumesmar *et al*., 1995). However, unlike oligodendrocyte precursors, Schwann cells express NCAM but not PSA. To overcome this obstacle, neonatal mouse Schwann cells were engineered to express sialyltransferase X (STX), one of the enzymes responsible for the polysialylation of NCAM (Angata and Fukuda, 2003). Ectopic expression of PSA enhanced cell motility *in vitro* (Lavdas *et al*., 2006) and improved axon regeneration *in vivo* after grafting in a mouse model of spinal trauma (Papastefanaki *et al*., 2007). These data showed that in rodents, Schwann cell behaviour can be modulated to promote CNS axon regeneration and functional repair without impinging on their myelination potential.

It is well-established that glial cell plasticity differs with age and that there is a close similarity of behaviour between monkey and human Schwann cells. In view of a clinical application, adult non-human primate Schwann cells, therefore, appear as an ideal tool to study any potential strategy explored previously in mice (Girard *et al*., 2005). In the present study, we asked whether conferring sustained expression of PSA to adult macaque Schwann cells promoted their migration and mixing with sister Schwann cells, astrocytes and white and grey matter *in vitro*. Moreover, since migration is a major issue for Schwann cell-based therapy in multiple sclerosis, we assessed the effect of PSA forced expression on Schwann cell migration through normal CNS, grafting cells remotely from a demyelinated lesion targeted to the dorsal spinal cord. For obvious ethical reasons, we addressed this first by grafting adult macaque Schwann cells in mice, rather than directly in non-human primates (Girard *et al*., 2005). Finally, while in models of spinal cord trauma, the effect on myelin repair can hardly be dissociated from an effect on

neuroprotection and/or regeneration, we also investigated whether ectopic expression of PSA in adult macaque Schwann cells resulted in improved remyelination of the demyelinated lesion.

Material and methods

Cell culture

Adult primate Schwann cells

Schwann cells were purified from sural nerve biopsies of adult *macaca fascicularis* as described earlier (Avellana-Adalid *et al*., 1998). Purified Schwann cells (95%, S100 positive) were maintained in proliferation medium containing 90% Dulbecco's Modified Eagle Medium (Invitrogen, Cergy-Pontoise, France), 10% foetal calf serum (Invitrogen, Cergy-Pontoise, France), 1 μg/ml forskolin (Sigma, St Louis, MO, USA), 10 ng/ml human heregulin β1 (RetD system) and 10 μg/ml insulin (Sigma).

Neonatal rat astrocytes

Primary astrocytes were purified from neonatal rat (P1) cortex as described by McCarty and de Vellis (1980). Briefly, the cerebral cortices were freed of meninges, collected in Dulbecco's Modified Eagle Medium containing 10% foetal calf serum and dissociated by passage through a serological pipette. The mixture was filtered through 70 μm nylon mesh, centrifuged, resuspended in the Dulbecco's Modified Eagle Medium and then plated onto poly-L-lysine-coated culture flasks. After one week, microglia and progenitor cells were removed by shaking, and astrocyte purity assayed by glial fibrillary acidic protein (GFAP) immunostaining.

Construction of expression vector pSTX-GFP-N3

The coding region of the mouse STX (ST8SiaII) cDNA (gift from Dr Shuichi Tsuji, RIKEN, Wako Saitama, Japan) was amplified by PCR with oligonucleotide AAGCTTCGAATTCAGGCAGGGCA GGATGCAGCTGCAGTTC as forward primer and with oligonucleotide CGGTACCGTCGACTGCAGAATTCTGCGTAGCCCCATCACA as reverse primer. This sequence was inserted by PCR in the pEGFP-N3 vector (Invitrogen, Cergy-Pontoise, France) upstream of the green fluorescein protein (GFP) sequence. The stop codon of the STX sequence was removed to obtain the fusion protein STX-GFP.

Construction of lentiviral vector HIV-CMV-STX-GFP and particle production

The coding sequence for STX-GFP, cloned in the pEGFP-N3 vector (aforementioned), was inserted in the pTrip-CMV-WPRE plasmid (Zennou *et al*., 2001). Using directed mutagenesis, we inserted two restriction sites (SpeI and XhoI), which allowed the insertion of STX-GFP in the multiple cloning site of pTrip-CMV-WPRE plasmid. Lentiviral particles were produced by triple co-transfection of 293T cells with the pTrip-CMV-STX-GFP, envelope and encapsidation plasmids as described earlier (Charneau *et al*., 1992). Viral supernatants were concentrated by ultracentrifugation and quantified by P24 antigen enzyme-linked immunosorbent assay.

Schwann cell transfection and transduction

Transfected cells were used for the *in vitro* studies. For the *in vivo* experiments, we used transduced cells to obtain a steady and longer expression of PSA-NCAM.

Transfection

Schwann cells (2×10^6) were transfected by electroporation (Amaxa, Cologne, Germany) with 5 μg of the plasmid pSTX-GFP-N3 or pEGFP-N3 (control) according to the Amaxa protocol.

Transduction

To combine steady PSA expression and cell tracking *in vivo*, adult macaque Schwann cells (5×10^4) were first transduced with 12 ng p24 of HIV-CMV-GFP, which allowed strong and stable cytoplasmic GFP expression in Schwann cells and therefore, their unambiguous tracing after grafting (Bachelin *et al*., 2005; Girard *et al*., 2005). Expression of GFP was detected 48–72 h post-transduction. GFP expressing Schwann cells were either used as the control Schwann cells (Ct-SC) or subsequently transduced with the HIV-CMV-STX-GFP vectors (100 ng p24) as the sialyltransferase expressing Schwann cell (STX-SC) group. Since the STX-GFP expression was restricted to the Golgi, it was not easily detectable *in vivo*. Therefore, we had to use double-transduced Schwann cells with both the HIV-CMV-GFP and HIV-CMV-STX-GFP. PSA expression in modified Schwann cells was verified by immunostaining.

Cell–cell adhesion

To analyse intercellular adhesion, Schwann cells were trypsinized, resuspended in conical centrifuge tubes of 15 ml in proliferation medium at a density of 500 cells/μl and incubated at 37°C for 30 min. Then 60 μl of this cell suspension was seeded on coverslips and the number of cells isolated or forming aggregates was counted. Three independent experiments with a minimum of 12 fields per condition were quantified.

Schwann cell migration analysis by time-lapse video microscopy

To analyse global migration, the scratch migration assay (Meintanis *et al*., 2001) was used. Schwann cells were plated on poly-L-lysine coated coverslips at high density (100 000 cells/cm^2) and left for 24 h in proliferation medium. A gap of ~1 mm wide was generated by scratching the cell monolayer with a sterile tip. To analyse isolated Schwann cells motility, cells were plated at low density (5000/cm^2) on poly-L-lysine coated coverslips. For both assays, medium was changed and aphidicholin (10 μM, Sigma) was added to suppress cell movements resulting from cell proliferation. Cultures were transferred to a Zeiss inverted microscope equipped with a digital camera and the Metamorph image acquisition software. Migration of Schwann cells was monitored microscopically by acquiring digital images every 20 min for a period of 12 h under a 10× objective. For global migration, the distance of migration was obtained by measuring the area of repopulation of the gap between the time the scratch was generated (*T*0) and 6 and 12 h thereafter, using the ImageJ software. To measure migration of isolated Schwann cells, they were tracked for a period of 6 and 12 h using the Metamorph software.

Distance from origin was measured, and 60 cells were evaluated for each experimental condition. For each assay, three independent experiments with a minimum of three coverslips per condition were performed.

Schwann cell–astrocyte confrontation assay

Schwann cells and astrocytes were plated (5×10^4 cells/10 μl) on poly-L-lysine-coated cover slips and were separated by a 0.3 mm silicone stripe. After adhesion, the silicone stripe was removed, allowing confrontation of Schwann cells and astrocytes. The location of the silicone stripe was marked as the front line. Six days after plating, cells were fixed for immunocytochemistry using anti-p75 to identify Schwann cells, anti-PSA to identify STX-SC and anti-GFAP to identify astrocytes. The degree of Schwann cell–astrocyte overlap was quantified by measuring GFAP-positive ($GFAP^+$) area within the Schwann cell-positive area using ImageJ software. Each overlapping area was divided in to nine equivalent narrow stripes extending away from the front line (stripe 1, the closest and stripe 9, the furthest). The index of integration representing the amount of $GFAP^+$ area in the STX-SC area over that of controls was calculated for each stripe. Three independent experiments with four coverslips per condition were analysed.

Immunocytochemistry

Cell cultures were fixed in 2% paraformaldehyde for 10 min at room temperature and incubated with the primary antibody diluted in blocking solution—phosphate buffered saline—4% bovine serum albumin (Sigma), or 1 h at room temperature. Intracellular antigen permeabilization was achieved by incubating primary antibody with Triton 0.25%. Anti human p75 (1/250, Sigma) and anti S100 (1/100, Dako, Glostrup, Denmark) antibodies were used to characterize adult primate Schwann cells, anti-Galc antibody (mouse IgG3 hybridoma) (Ranscht *et al*., 1982), anti-O4 antibody (mouse IgM hybridoma) (Sommer and Schachner, 1981), identify pro-myelinating Schwann cells and anti-GFAP (1/100, Dako), to stain astrocytes. PSA expression by STX-GFP-Schwann cells was verified using mouse anti-PSA antibody (1/400, Abcys, Paris, France). Secondary fluorescein isothiocyanate or rhodamine conjugated antibodies, used to detect primary antibodies, were incubated 1 h at room temperature (Dako or Southern Biotechnology). Cell nuclei were labelled with Hoechst 33 342 (10 μg/ml, Sigma). Coverslips were mounted with fluoromount G (Southern Biotechnology, Alabama, USA) and evaluated using a DBM Leica fluorescence microscope and Explora Nova (La Rochelle, France) image acquisition software.

In vitro statistical analysis

Statistical analysis was performed using the SigmaStat software and the Student's *t*-test with $P<0.01$ for significance in all assays except for time-lapse video microscopy. The latter was performed using the Student's *t*-test with $P<0.05$ for significance. Statistical analysis of isolated Schwann cell motility was performed using one-way analysis of variance (ANOVA) with $P<0.05$ for significance.

Demyelination and Schwann cell transplantation

Animals

Three-month-old nude mice were purchased from JANVIER (Le Genest St Isle, France). All animal protocols were performed in accordance with the guidelines published in the National Institute of Health Guide for the Care and Use of Laboratory Animals.

Lesions

Mice were anaesthetized with a ketamine/xylazine mixture. Demyelination was induced by stereotaxic injection of lysophosphatidylcholine (LPC, 1%, 2 μl, Sigma) in 0.9% NaCl. LPC was injected (1 μl/min) into the spinal cord at the level of T8–T9 in the dorsal column white matter using a glass micropipette. The site of injection was marked with charcoal.

Grafts

Forty-eight hours after demyelination Schwann cells (2 μl of a 5×10^4 cells/μl suspension) transduced with the lentiviral vector encoding GFP (Ct-SC) or STX-GFP (STX-SC) were grafted onto the dorsal column white matter using a glass micropipette at a distance of one intervertebral space caudal to the lesion site.

Immunohistochemistry

Animals were sacrificed sequentially at 7-, 14- and 28-days post-transplantation (d.p.t.) with lethal doses of ketamine/xylazine and were perfused intra-cardially with 0.1 M phosphate buffer followed with 2% paraformaldehyde. Spinal cords were cryoprotected overnight in 20% sucrose, frozen and 10 μm thick sagittal sections serially cut. For immunohistochemistry, primary antibodies were as follows: polyclonal anti-GFAP (1/300, Dako) to identify astrogliosis; monoclonal anti-PSA-NCAM (1/400, Abcys) to identify STX-SC; monoclonal anti myelin protein zero [P0; 1/5, hybridoma, (Yoshimura *et al*., 1996)] to detect peripheral nervous system myelin; monoclonal anti-myelin oligodendrocyte glycoprotein (MOG: 1/200, ascite obtained from Dr Linnington, Edinburgh, UK) to detect CNS myelin; polyclonal anti-Caspr (1/800, generous gift from E. Peles, Rehovot Israel) to identify paranodes; monoclonal anti-PAN-Na_v (1/100, Sigma) to detect sodium channels; and polyclonal anti-laminin (1/200, Sigma) to identify the extracellular matrix and blood vessels. Following primary antibodies, sections were incubated with appropriate secondary antibodies conjugated with rhodamine (red) or aminomethylcoumarin acetate (blue). Sections were analysed under a dual-beam Leica fluorescent microscope using Explora Nova image acquisition software.

Electron microscopy analysis

For electron microscopy analysis, animals were perfused with 4% paraformaldehyde and 0.025% glutaraldehyde (Electron Microscopy Science, Hatfield, USA). Spinal cords were removed and cut in 100 μm slices on a vibratome VT-1000S (Leica microsystems, Wetzlar, Germany). Slices were incubated overnight with anti-GFP (1/100) at 4°C and rinsed three times. Spinal cord sections were incubated for a 3 h at room temperature with biotin-conjugated anti-rabbit antibody (1/100, Amersham, Buckinghamshire, UK), rinsed three times and incubated for a further 3 h with streptavidin-conjugated to β-galactosidase (1/100, Vector, Burlingame, UK). β-Galactosidase presence was revealed with Bluo-Gal (Sigma) staining. Immuno-

labelled slices were then post-fixed with 2.5% glutaraldehyde for 2 h and 2% osmium tetroxide (Electron Microscopy Science) for 30 min. After dehydration, slices were embedded in epon. Ultra-thin sections were cut using an ultra-microtome and were viewed using Philips electron microscope.

In vivo quantification and statistical analysis

Post-mortem evaluation was performed on 8–14 animals in each group/time-point using the ImageJ software. Longitudinal migration was established measuring the longest distance between the most caudal and the most rostral GFP positive (GFP^+) Schwann cells on two spinal cord sections spaced by 50 μm for each animal.

Evaluation of Schwann cell recruitment by the lesion was performed on 18 sections spaced by 40 μm for each group of animals. For each lesion, the GFP^+ area and the lesion area, defined by MOG staining, were measured. The GFP^+ area was expressed as a ratio of the lesion area. The limits of the lesions were defined scanning sections at 20×.

Evaluation of GFP–Schwann cell interaction with $GFAP^+$ astrocytes in the graft site was performed measuring the percentage of GFP^+ areas present in $GFAP^+$ area:

$$\frac{(GFP^+\text{area in } GFA^+\text{area} \times 100)}{\text{Total } GFP^+\text{area}}$$

For each animal, eight sections spaced by 70 μm were quantified. Results are presented as the distribution of animals with low (<60%) or high (>60%) GFP^+ Schwann cell overlap with $GFAP^+$ area. P0 immunoreactive internodes were quantified according to McTigue *et al*. (1998) scanning the lesion area at 40×. The extent of exogenous Schwann cell remyelination was quantified measuring the area of co-localization of P0 and GFP per lesion. The extent of endogenous Schwann cell remyelination was quantified measuring the area of P0 staining, not co-localized with GFP positivity. As endogenous remyelination by oligodendrocytes is characterized by shorter internodes, which can be identified by Caspr staining of paranodes (Lasiene *et al*., 2008), the extent of endogenous remyelination by oligodendrocytes was quantified measuring the area of MOG staining associated with tightly packed $Caspr^+$ internodes. For each animal, 12 sections spaced by 8 μm were quantified.

Statistical analysis was performed using the Student's *t*-test with $P<0.01$ for significance using SigmaStat software. Assessment of Schwann cell recruitment by the lesion was performed using a rank Gehan–Breslow statistical test ($P<0.05$), considering the presence (or absence) of GFP^+ Schwann cells at the lesion and the quantity of GFP^+ area at the lesion site.

Results

Expression of NCAM and PSA-NCAM by transduced Schwann cells *in vitro*

Immunocytochemistry for NCAM and PSA-NCAM showed that like in the neonate rodent, adult macaque Schwann cells expressed NCAM (Fig. 1A) but not PSA-NCAM (Fig. 1B). To force expression of PSA in Schwann cells, they were purified and transduced with the STX or control lentiviral vector. Schwann cells were transduced with an efficiency of 73 ± 3%. This was confirmed by immunohistochemistry for PSA-NCAM, which showed that 75 ± 4% of the STX-SC expressed PSA-NCAM (Fig. 1C) while none of the Ct-SC did (Fig. 1B). Transduced STX-SC expressed PSA-NCAM strongly on their membrane, while expression of STX-GFP protein was restricted to the Golgi, the expected location of the sialyltransferase. Thus, the enzyme activity and localization were not affected by its fusion with GFP. This expression was stable since PSA and STX expression lasted *in vitro* for up to 6 months in the majority of transduced Schwann cells. Treatment with endoN showed that PSA was no longer expressed on the Schwann cells membrane while STX-GFP remained expressed in the Golgi (Fig. 1D). Since EndoN cleaves PSA specifically on NCAM, these results confirm that STX specifically sialylates NCAM in transduced macaque Schwann cells.

Characterization of STX overexpressing Schwann cells *in vitro*

To determine whether transduction would modify the antigenic phenotype of Schwann cells, cultures were labelled by immunohistochemistry for cell stage specific markers (Supplementary Fig. 1). In proliferating medium, 98 ± 1% of Ct-SC and 97 ± 2% STX-SC expressed p75 (Supplementary Fig. 1A and B) and S100 (Supplementary Fig. 1C and D), antigens expressed by all Schwann cell stages. Few cells (<1%) expressed galactosylceramidase or the glial progenitor O4, markers of mature Schwann cells (Jessen and Mirsky, 2005) (not shown). After 5 days in differentiation medium (Bachelin *et al*., 2005), the number of galactosylceramidase and O4 expressing Schwann cells increased equally in Ct-SC and STX-SC groups, with 29 ± 2% and 33 ± 6% for galactosylceramidase-expressing Schwann cells (Supplementary Fig. 1E and F), and 25 ± 6% and 22 ± 0.5% for O4 expressing Schwann cells, respectively (Supplementary Fig. 1G and H). Quantification of the number of 5-bromo-2-deoxyuridine positive Schwann cells indicated that both cell types proliferated equally well after transfection or transduction (data not shown).

We tested the possibility that forced expression of PSA on SC membranes would modulate SC self-adhesive properties. Ct-SC and STX-SC were dissociated and maintained in suspension for 30 min. Figure 2 shows that Ct-SC formed small aggregates (Fig. 2A), while the majority of STX-SC remained dispersed as single cells (Fig. 2B). Quantification of the number of SC remaining isolated versus those forming aggregates (of variable sizes) within 30 min of playing, showed that the number of isolated cells was significantly higher (1.6-fold) in STX-SC that the Ct-SC ($P<0.05$). On the other hand, the number of cells forming large aggregates was significantly higher (9.6-fold) in the Ct-SC compared to STX-SC ($P<0.001$). This indicates that ectopic expression of PSA decreased SC-SC interactions.

The principal aim of this study was to investigate whether forced expression of PSA improved adult macaque Schwann cell migration ability. The scratch assay was used as global assessment of Schwann cell ability to repopulate a cell-free area in a given time (Meintanis *et al*., 2001). Schwann cells were plated at high density, each monolayer was scratched 24 h post-plating and repopulation was allowed on the scratched area for 12 h. Six hours after plating, quantitative analysis of the repopulated

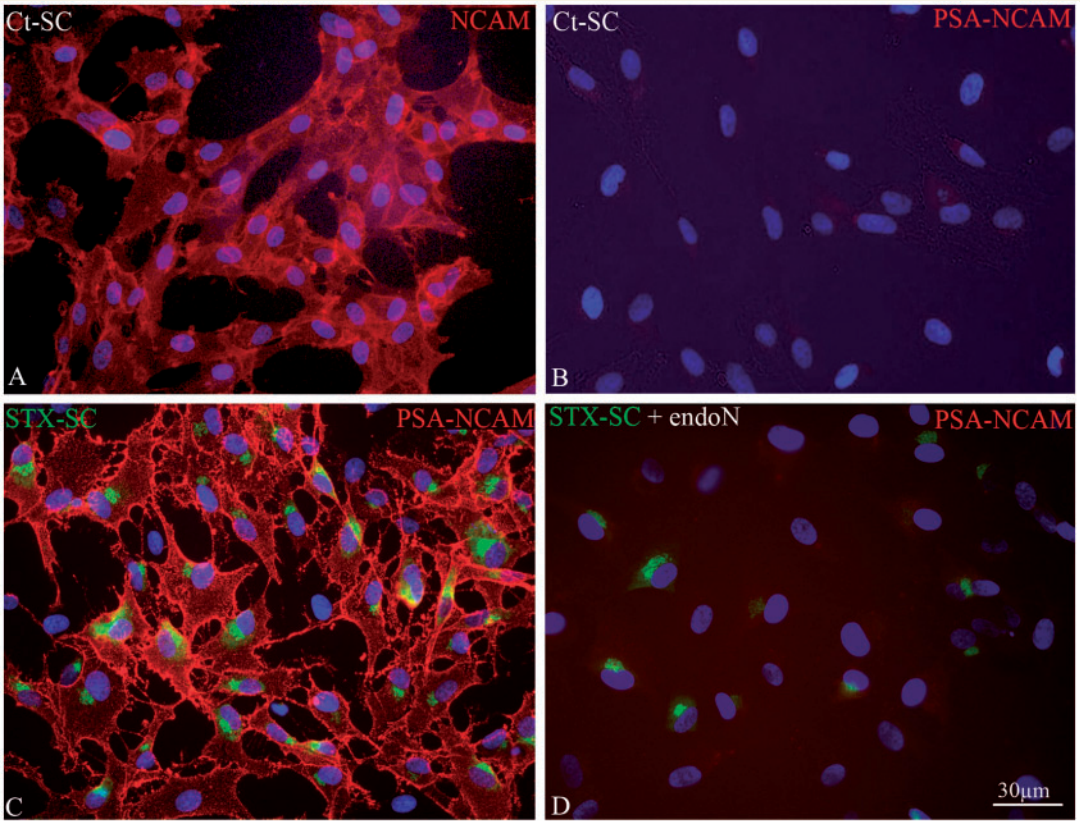

Figure 1 *In vitro* expression of NCAM and PSA-NCAM by adult macaque Schwann cells. Ct-SC express NCAM (**A**) but not PSA-NCAM (**B**). STX-SC strongly express PSA-NCAM (**C**, red) on their membrane, while STX-GFP (**C**, green) expression is restricted to the Golgi, the location of sialyltransferase activity. After treatment with endoN, which specifcally cleaves PSA on NCAM, PSA is no longer expressed on the Schwann cell membrane (red, **D**) while STX-GFP is still present in the Golgi (green, **D**).

area by video microscopy showed that STX-SC (Fig. 3B) repopulated the scratched area significantly faster than Ct-SC ($P<0.05$) (Fig. 3A and C).

To analyse the migration potential of individual Schwann cells (and thus independently of any mutual interactions), they were plated at low density and the progression of single cells followed by video microscopy. Evaluation of the shortest distance between the origin and arrival points of each cell showed that STX-SC migrated 1.4- and 1.7-fold further than Ct-SC at 6 and 12 h, respectively ($P<0.05$) (Fig. 3D).

Migration of Schwann cells grafted in the CNS is largely compromised by their exclusion from astrocytes (Lakatos *et al*., 2003). This phenomenon can be reproduced *in vitro* with the Schwann cell–astrocyte confrontation assay (Wilby *et al*., 1999). To investigate whether forced expression of PSA modulated this failed interaction, macaque Ct-SC and STX-SC cells were confronted to rat astrocytes for 6 days, and the Schwann cell frontline was marked at plating time (Fig. 4A–C). Immunolabelling for p75 and GFAP to detect Schwann cells and astrocytes, respectively, showed that the integration of the two populations was much improved in the STX-SC group when compared with the Ct-SC group. Interestingly, astrocytes invaded Schwann cells but the reverse did not occur. Quantification of the degree of integration of $GFAP^+$ among $p75^+$ Schwann cells confirmed that Schwann cells–astrocyte interaction was significantly more prominent with STX-SC compared with Ct-SC with up to a 1.6-fold increase in the most distant stripes from the front line (stripe 7–9, Fig 4D) ($P<0.05$).

Schwann cell transplantation in the demyelinated spinal cord

Migration and recruitment of the grafted Schwann cells

To investigate the ability of adult macaque Schwann cells to integrate and migrate in the CNS *in vivo*, LPC-induced demyelination was targeted to the spinal cord dorsal funiculus of nude mice. Next Ct-SC ($n=40$) and STX-SC ($n=40$) were grafted caudally in the same tract, at a distance of one intervertebral space ($d=2$ mm) from the LPC-injected site. Grafted animals in each group were sacrificed at 7 ($n=20$) and 28 ($n=20$) d.p.t.

The spatio-temporal distribution of the grafted Schwann cells highlighted differences between the Ct-SC and STX-SC groups. Detection '*in toto*' of GFP under the fluorescent dissecting microscope (Supplementary Fig. 3), showed that at 7 d.p.t. (Supplementary Fig. 3A and C) and 28 d.p.t. (Supplementary

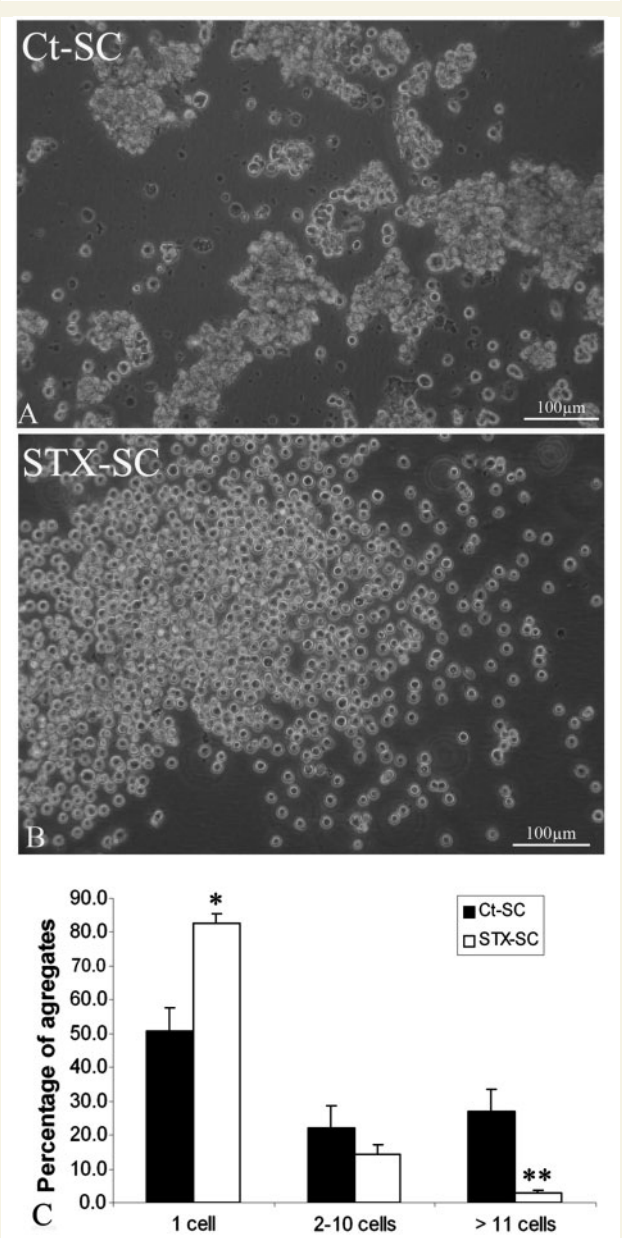

Figure 2 Effect of PSA-NCAM expression on inter-Schwann cell interaction *in vitro*. Visualization of Ct-SC **(A)** and STX-SC **(B)** 30 min after dissociation in single cell suspensions. Ct-SC form small aggregates **(A)** while STX-SCs remain dispersed as a cloud of single cells **(B)**. **(C)** Quantification of the percentage of Schwann cells remaining isolated or forming aggregates of variable sizes after 30 min of plating. Student's *t*-test $*P<0.05$, $**P<0.001$. Error bars represent SEM.

Fig. 3B and D), the majority of GFP$^+$ Schwann cells were found at the graft point in both groups of animals. However, the presence of cells in the graft-lesion intermediate zone and in the lesion differed between the two groups of animals. In the STX group, GFP$^+$ Schwann cells were detected in the intermediate zone and at the lesion site in the majority of the STX-SC animals at 7 and 28 d.p.t., whereas in the Ct-SC group, GFP-Schwann cells that were localized in the intermediate zone and the lesion site were found only in a minority of the transplanted animals. The ability of Schwann cells to migrate was further assessed on longitudinal frozen sections by scanning sections for GFP throughout the spinal cord. Quantification at 7 d.p.t. confirmed that the longest distance of migration of GFP$^+$ cells (Fig. 5C) was significantly greater in the STX-SC (Fig. 5A) group than in the Ct-SC group (Fig. 5B). Next, we analysed whether ectopic expression of PSA by Schwann cells promoted their ability to be recruited by the lesion. More cells were found at the lesion site in the STX-SC group (Fig. 5F and G) compared with the control group (Fig. 5D and E). Quantification of GFP positivity per lesion area (Fig. 5H), showed that ectopic expression of STX improved significantly ($P<0.05$) and of 3-fold Schwann cell recruitment by the lesion at 7 and 28 d.p.t.

Interface of grafted Schwann cells with astrocytes and myelin

To gain more insight into the consequence of PSA-NCAM ectopic expression on Schwann cell behaviour *in vivo*, Schwann cell interface with the host environment was fully analysed 7 d.p.t. Since Schwann cells and astrocytes are mutually exclusive, we analysed the intermingling of the grafted adult macaque Schwann cells with the host astrocytes. Immunohistochemistry for GFAP showed that astrogliosis occurred in the two groups of animals within the graft (Fig. 6A and C), in the intermediate zone and at the lesion site at any given experimental time (data not shown). Evaluation of the amount of GFP$^+$ area overlapping with the GFAP$^+$ area (Santos Silva *et al*., 2007), showed that STX-SC (Fig. 6D) had a greater propensity to integrate GFAP$^+$ areas than Ct-SC (Fig. 6B), with high integration in 25% of animals in the control group and in 60% of the animals in the STX group. These results confirm the greater ability of STX-SC over Ct-SC to interact with astrocytes *in vitro*.

Since Schwann cells do not migrate along myelinated tracts when grafted in the adult spinal cord (Baron-Van Evercooren *et al*., 1992), we also questioned their ability to do so when expressing PSA-NCAM. Double immunohistochemistry for GFP and MOG showed that neither Ct-SC nor STX-SC were present in MOG$^+$ myelin in the graft (data not shown), intermediate zone (Fig. 7) or lesion (Fig. 5D and F). As a result, migrating Schwann cells were confined to the dorsal midline (Fig. 7B–F). While Ct-SC migrated as single cells, STX-SC often migrated in rows reminiscent of chain-like migration. Combined immunodetection of laminin and GFP showed that Schwann cells associated preferentially with the extracellular matrix of small blood vessels nested in the dorsal midline (Fig. 7B and E).

Finally, we investigated whether the greater propensity of STX-GFP-Schwann cells to integrate and migrate in the CNS was correlated with PSA expression by the grafted Schwann cells. Immunohistochemistry for PSA showed that only STX-SC expressed PSA. This expression was transient, since PSA was clearly detected at 7 d.p.t. (Fig. 8A and C), but was weaker at 14 d.p.t. (Fig. 8D and F) and no longer detectable by 28 d.p.t. (data not shown).

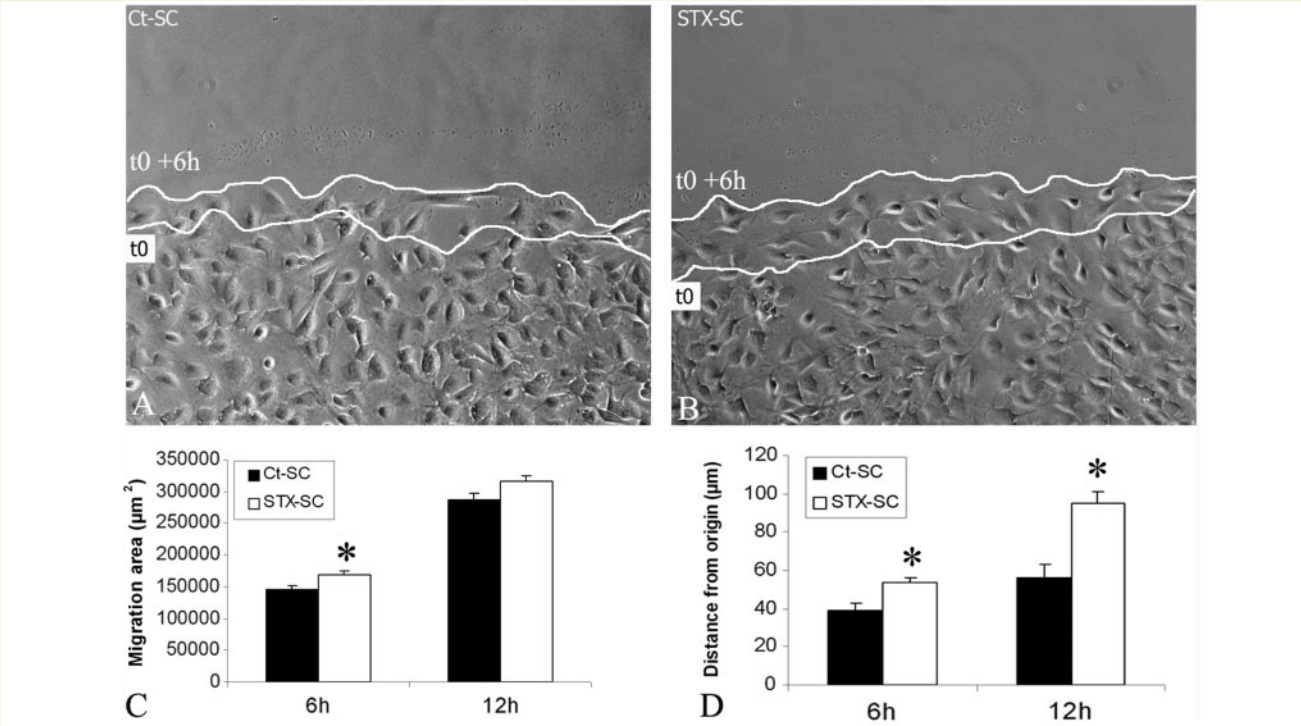

Figure 3 Effect of PSA-NCAM expression on Schwann cell migration *in vitro*. Confluent Schwann cell monolayers were scratched and subsequent migration into the gap visualized by video microscopy after 6 and 12 h of plating. STX-SC **(B)** repopulated the scratched area more rapidly than Ct-SC **(A)**. Quantification of the global area of migration of Ct-SC and STX-SC **(C)**, or of the distance of migration of the individual Schwann cells from their origin to arrival **(D)** showed that STX-SC migrated more efficiently than Ct-SC. Student's *t*-test $*P < 0.05$. Error bars represent SEM. White lines indicate Schwann cell front lines at onset (*t*0) and 6 h later (*t*0 + 6 h).

Remyelination potential

Remyelination of LPC-induced lesions starts at 7 d.p.t. and is nearly completed by 28 d.p.t. (Gout *et al*., 1988; Jeffery and Blakemore, 1995). It is achieved by endogenous oligodendrocyte precursors but also by Schwann cells (reviewed in Zujovic *et al*., 2007). We first investigated whether transplanted Ct-SC and STX-SC participated in the lesion repair by producing newly formed myelin and whether ectopic expression of PSA could promote this process. The relative abundance of peripheral versus CNS remyelination within the margins of the lesion, was evaluated by immunohistochemistry for P0 (Fig. 9A and B) and MOG (Fig. 9E and G) to detect peripheral and central myelin, respectively. Quantification of P0 (Fig. 9F) and MOG immunoreactivity in the lesion showed equal amounts of total peripheral (Ct-SC = 0.09 ± 0.03; STX-SC = 0.13 ± 0.08 $\mu m^2/\mu m^2$ of lesion) and central (Ct-SC = 0.301 ± 0.07; STX-SC = 0.310 ± 0.08 $\mu m^2/\mu m^2$ of lesion) myelin for each group. To establish the relative contribution of Ct-SC and STX-SC to exogenous remyelination, the amount of P0 co-localized with GFP was quantified. $GFP^+/P0^+$ myelin-like figures were detected in STX-SC grafted animals only (Fig. 9B) and represented 5% of the global Schwann cell remyelination process (Fig. 9C). These data indicate that only STX-SC, which arrived in the lesion faster, were able to out-compete endogenous myelin-forming cells for remyelination. The presence of exogenous newly formed myelin was further confirmed by electron microscopy revealing the presence of GFP with BluoGal precipitates. Figure 9D illustrates the presence of BluoGal precipitates in myelin with specific peripheral myelin features such as the 1:1 association of Schwann cell with axon and the presence of a basal membrane around the compacted myelin (Fig. 9D, inset). Finally, we questioned the functionality of STX-SC-derived myelin focusing on the ability to re-assemble paranodal Caspr and nodal voltage-gated Na_v proteins, as endogenous Schwann cells do (Black *et al*., 2006). Immunodetection of Caspr, and/or Na_v in association with P0 and GFP, showed that $P0^+/GFP^+$ STX-SC internodes were clearly associated with Na_v channels flanked by $Caspr^+$ paranodes at the node level (Fig. 9E–G). STX-SC lead to the reconstruction of well-organized internodes on host axons throughout the lesion with a very similar expression pattern to that observed for endogenous Schwann cells.

Discussion

It has been previously demonstrated in rodents and macaques that Schwann cells can efficiently remyelinate CNS axons after transplantation in the demyelinated spinal cord. However, their therapeutic efficacy is limited due to their poor migration potential. Therefore, promoting Schwann cell migration appears as a

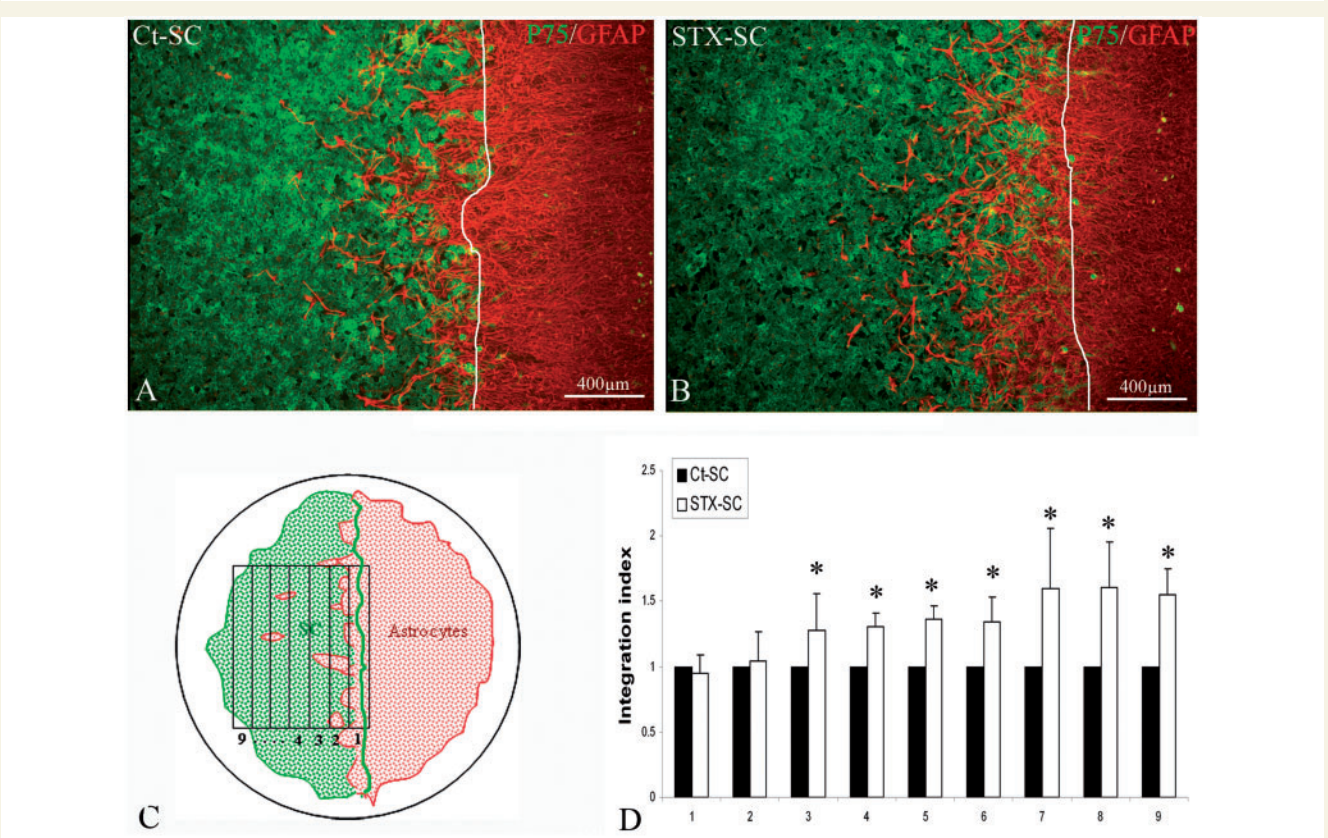

Figure 4 Effect of PSA-NCAM expression on Schwann cell–astrocyte interactions *in vitro*. Astrocytes and Ct-SC or STX-SC were plated at opposite sides of a silicon strip, and populations allowed to merge for 6 days after silicone removal. Schwann cell–astrocyte interaction was evaluated by immunohistochemistry for p75 to detect Schwann cells, and GFAP to detect astrocytes in Ct-SC **(A)** and STX-SC **(B)** cultures. Astrocyte integration among Schwann cells was more prominent in the STX-SC cultures than Ct-SC. The degree of Schwann cell–astrocyte overlap was quantified measuring $GFAP^+$ area in the Schwann cell-positive area. Starting from the Schwann cell frontline (white line, **A** and **B**), each overlapping area was divided in nine equivalent stripes as shown schematically in **(C)**. The amount of $GFAP^+$ area in the STX-SC area over that of Ct-SC shows that Schwann cell interaction with astrocytes was significantly higher in the STX-SC group compared to the Ct-SC group **(D)**. Student's *t*-test $*P < 0.05$. Error bars represent SEM.

promising strategy to improve CNS remyelination in diseases such as multiple sclerosis. Engineering neonatal mouse Schwann cells to overexpress PSA, enhanced their motility *in vitro* (Lavdas *et al*., 2006) and promoted CNS regeneration and functional repair after grafting in a mouse model of spinal trauma (Papastefanaki *et al*., 2007). To question whether such a strategy could be translated at a pre-clinical level for myelin diseases, we investigated whether ectopic expression of PSA-NCAM would be of benefit to promote remyelination by adult primate Schwann cells in the context of CNS demyelination. In this study, we have made three major observations: (i) *in vitro*, we show that ectopic expression of PSA not only promoted adult macaque Schwann cell migration and interaction with astrocytes, but also decreased their adhesion among sister cells; (ii) grafting Schwann cells remotely from focal demyelinated lesions targeted to the dorsal spinal funiculus, we provide *in vivo* evidence for improved integration of the grafted Schwann cells among reactive astrocytes, and enhanced migration through normal CNS along the dorsal midline; (iii) as a consequence, improved migration of the exogenous Schwann cells accelerated their recruitment to the lesion and enhanced their contribution to remyelination of the distant CNS lesions. These novel observations could have an important therapeutic implication if Schwann cells were to be used to promote myelin repair in multiple sclerosis.

Enhanced Schwann cell migration results from modified inter-Schwann cell interaction and enhanced integration of Schwann cells into an astrocyte rich area

In the present study, ectopic expression of PSA enhanced adult macaque Schwann cells migration *in vitro* in high and low confluent cultures, thus underlining the role of PSA in facilitating Schwann cell movement amongst each other and/or with their adhesive substrate (reviewed in Rutishauser, 2008). We showed that forced polysialylation of NCAM on Schwann cell membranes decreased inter-Schwann cell interactions *in vitro* preventing their self-aggregation in favour of single cell suspension. These

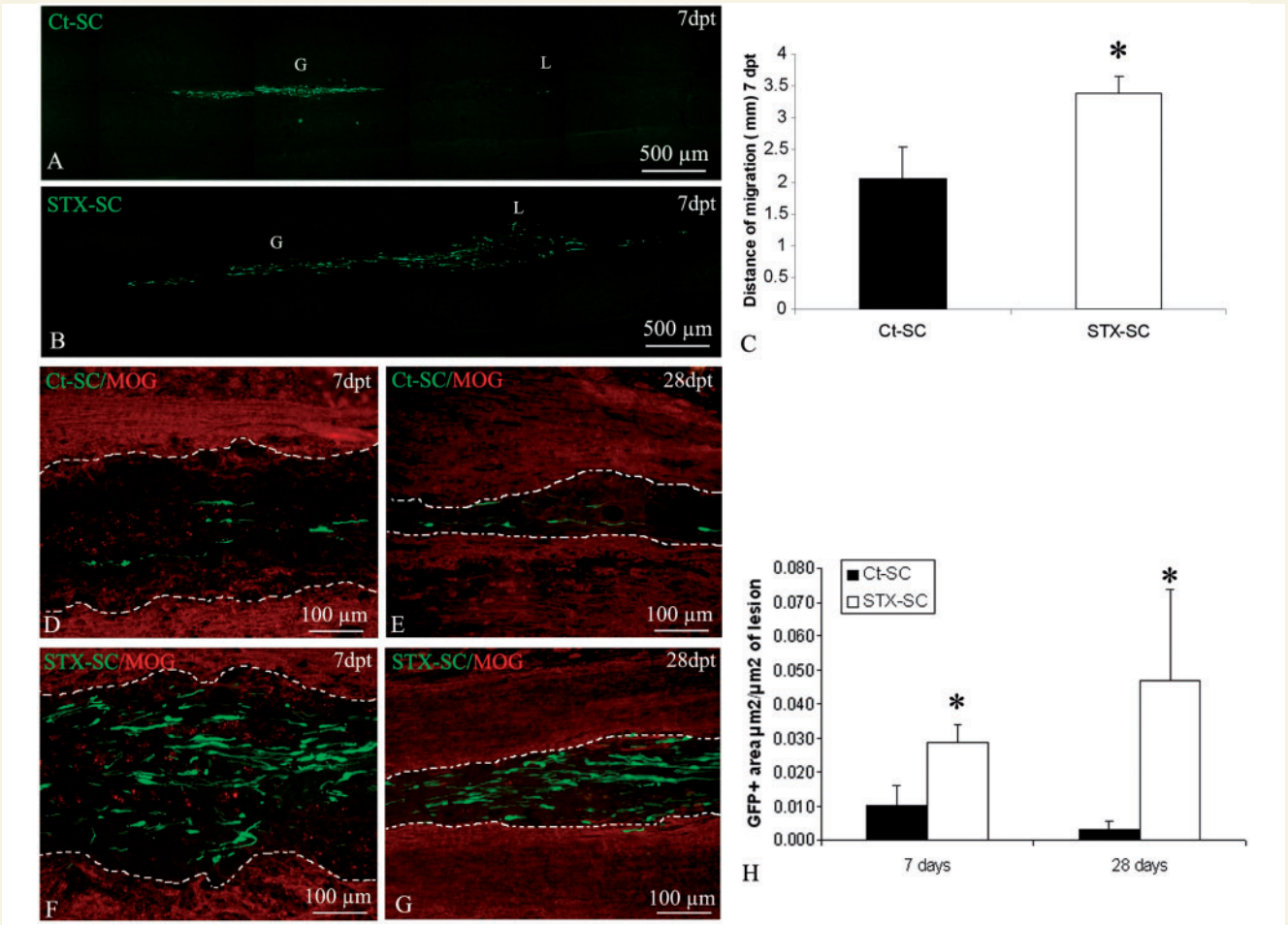

Figure 5 Migration and recruitment by the lesion of GFP-expressing Schwann cells. Sagittal frozen sections of spinal cords grafted with Ct-SC and STX-SC 7 d.p.t. illustrate improved migration of STX-SC **(B)** compared with Ct-SC **(A)**. Quantification of the longest distance of migration in the two groups of cells confirms that STX-SC migrate significantly faster than Ct-SC (Student's *t*-test $*P<0.02$) **(C)**. Consequently, Schwann cell recruitment by the lesion was more prominent in the STX-SC group **(F** and **G)** than in the Ct-SC group **(D** and **E)** at 7 **(D** and **F)** and 28 d.p.t. (**E** and **G). (H)** Quantification of the recruited Schwann cells at 7 and 28 d.p.t. confirms enhanced recruitment of STX-SC at all time points (Rank Gehan–Breslow statistical test with $P<0.05$). Error bars represent SEM. (in **A** and **B**, **G** indicates the graft and L, the lesion; in **D–G**, dotted lines indicate the margins of the lesion).

observations are in line with the finding that polysialylation of NCAM promoted inter-membrane repulsion, and was sufficient to overcome homophylic NCAM, or N-Cadherin attraction (Johnson *et al*., 2005). Since Schwann cells express NCAM (Lavdas *et al*., 2006) (present study) and N-Cadherin (Fairless *et al*., 2005), this effect could be of direct consequence on inter-Schwann cell fluidity and ability to migrate in the dish. Improved migration was further confirmed by grafting adult macaque Schwann cells remotely from a focal myelin lesion targeted to the dorsal spinal cord. The spatio-temporal distribution of Schwann cells in the dorsal funiculus argues in favour of accelerated migration rather than enhanced cell dispersion, since grafted cells were not observed outside this migratory path. Improved migration of STX-SC may thus have resulted from increased Schwann cell fluidity. However, recent findings indicated that NCAM polysialylation is also necessary for the directional response of neural or glial progenitors to a variety of growth factors (Glaser *et al*., 2007). Since grafted Schwann cells were attracted by the lesion (present study) and several growth factors are upregulated in response to spinal cord demyelination (Hinks and Franklin, 2000) similar mechanisms may have operated to enhance STX-SC migration and recruitment by the lesion. In fact, this would explain the minor effect of PSA on migration *in vitro* compared with migration *in vivo*.

Since astrocytes are known to play a major role in restricting Schwann cell migration in the demyelinated spinal cord (Blakemore and Franklin, 2000; Lakatos *et al*., 2003), we investigated the functional consequences of forced PSA-NCAM expression by adult macaque Schwann cells on their ability to intermingle with astrocytes. As for neonate mouse Schwann cells (Papastefanaki *et al*., 2007), PSA-NCAM expression by adult macaque Schwann cells reduced Schwann cell–astrocyte boundaries *in vitro*. Indeed, the modified interaction between the two cell types, resulting from PSA expression, was sufficient to allow

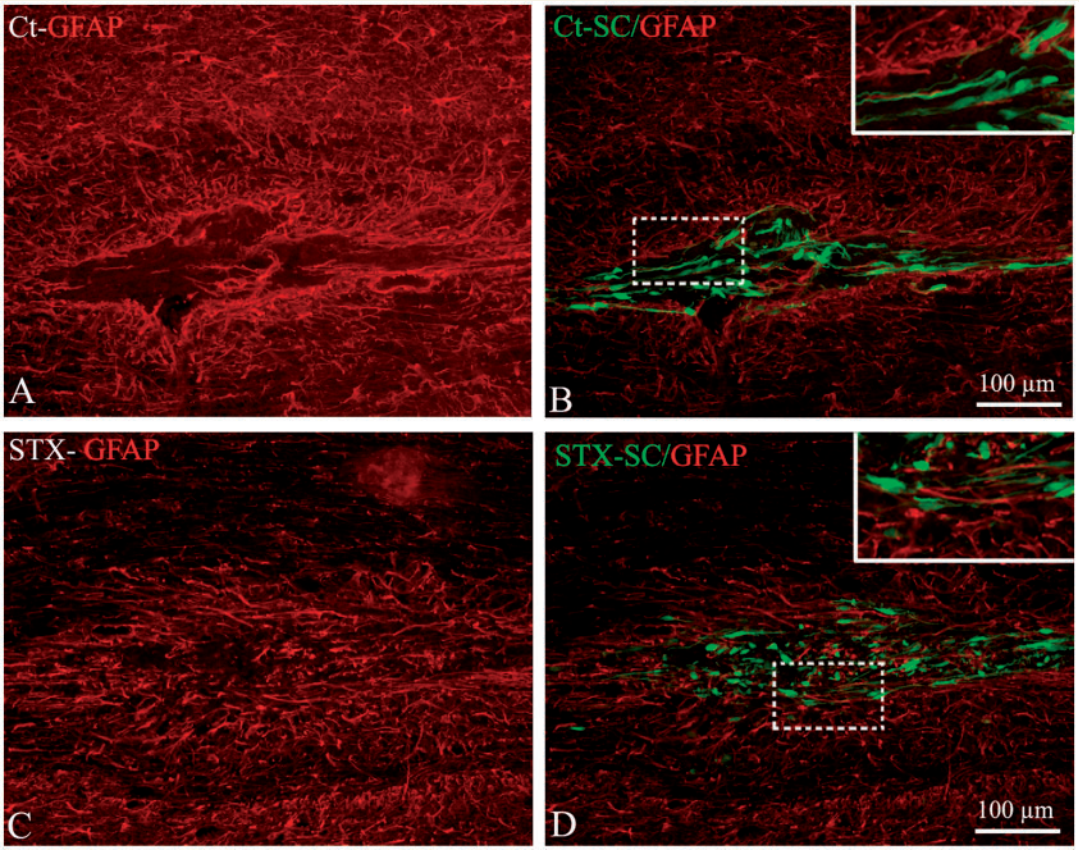

Figure 6 Effect of PSA-NCAM expression on Schwann cell–astrocyte interactions in the graft area. Immuno-labelling for GFAP (red) and GFP (green) shows a lack of GFAP immunoreactivity within the graft area of Ct-SC **(A** and **B)** but not STX-SC **(C** and **D)**. Higher magnification (inserts corresponding to the dashed box) illustrates improved interaction of STX-SC with astrocytes compared with Ct-SC.

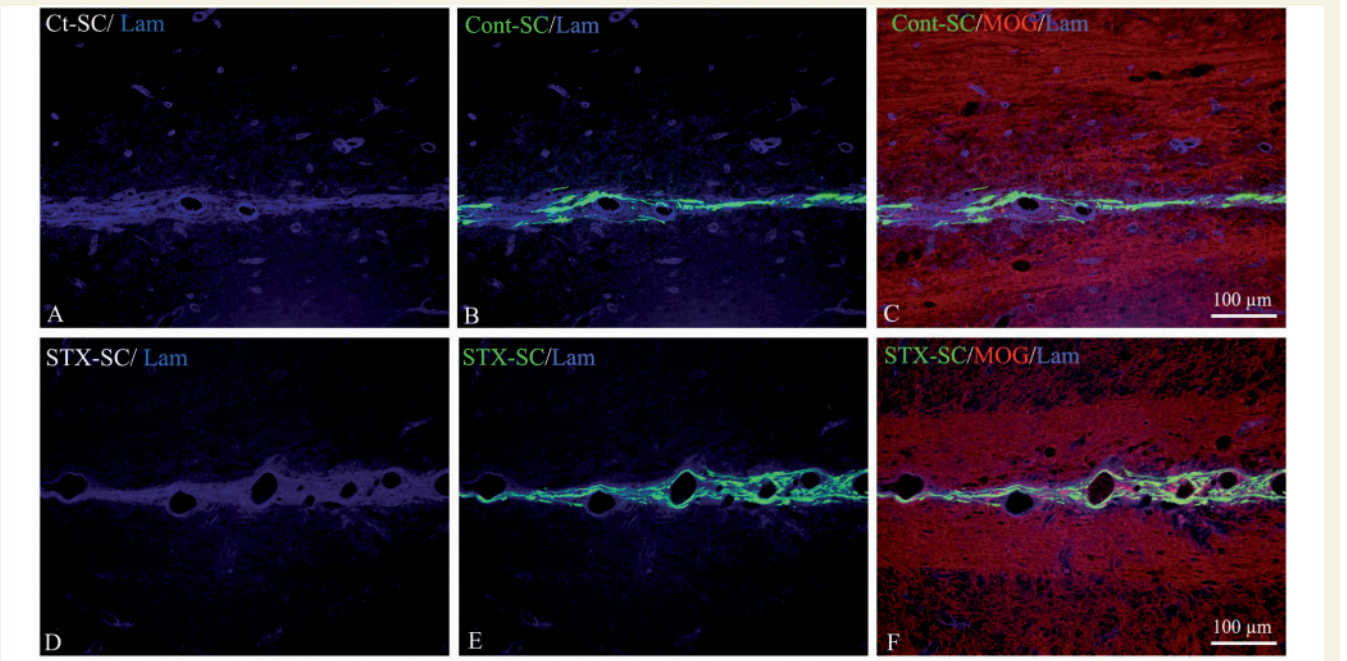

Figure 7 Effect of PSA-NCAM expression on the migratory pattern of grafted Schwann cells. Double labelling for MOG (**C** and **F**, red) and laminin (**A–F**, blue) in the intermediate zone shows that GFP expressing Ct-SC **(B** and **C)** and STX-SC **(E** and **F)** migrate along laminin$^+$ structures but not within MOG$^+$ myelin.

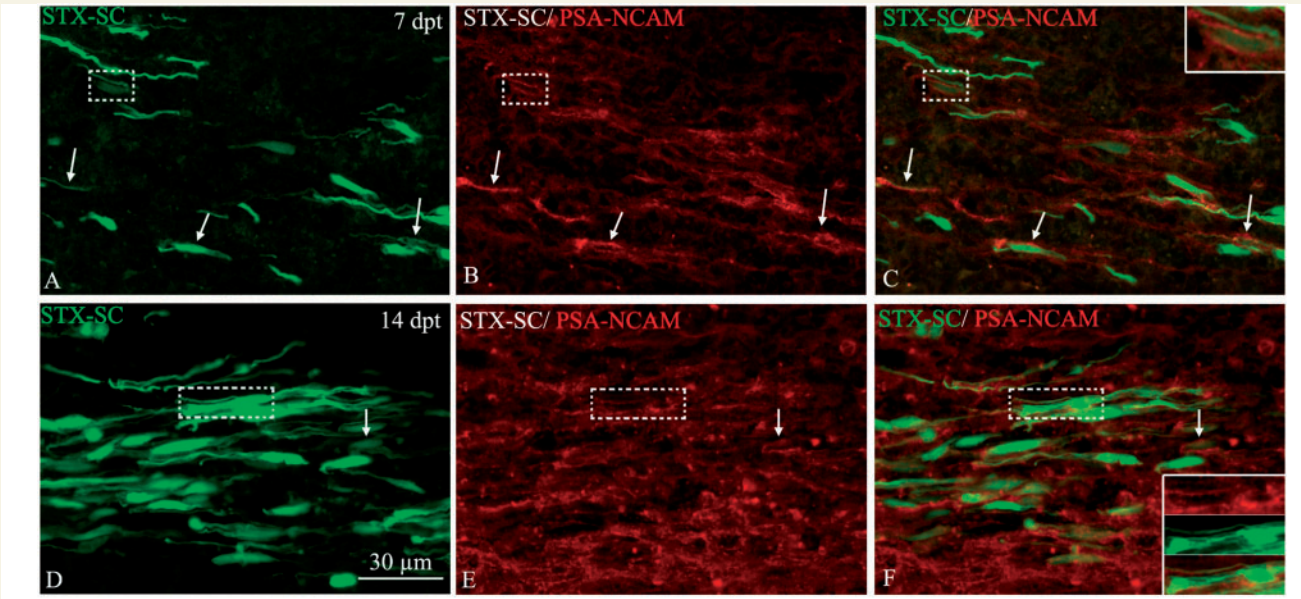

Figure 8 PSA NCAM expression by the grafted STX-SC. Double immuno-labelling of horizontal frozen sections for PSA-NCAM (red) and STX-SC (green). **(A–C)** At 7 d.p.t., the majority of STX-SC (arrows) express PSA-NCAM on their membrane. **(D–F)** Fourteen d.p.t., the number of STX-SC expressing PSA-NCAM (arrows) and PSA intensity is decreased. Inserts show higher magnifications of the dashed box areas illustrating double labelled cells.

Schwann cells and astrocytes to mix with each other *in vitro*. However, despite these *in vitro* observations, Papastefanaki and colleagues (2007) failed to detect any differences in astrogliosis *in vivo*, possibly due to insufficient PSA expression levels by the Schwann cells, or the presence of strong inhibitory cues present in spinal trauma lesions and absent in Schwann cell–astrocyte co-cultures. In agreement with their *in vivo* findings, we did not detect major differences in astrogliosis, as evaluated by GFAP expression between control and PSA-NCAM expressing cells. However, analysis of Schwann cell–astrocyte mixing at the graft site, when cells depart actively from the graft (7d.p.t.), highlighted improved integration of STX-SC and astrocytes compared to controls. The failure of STX-SC in reducing astrogliosis is consistent with the finding that the Schwann cell-induced stress response in astrocytes is mediated by Schwann cell-derived soluble factors (Santos-Silva *et al*., 2007) not cell-to-cell contact, and therefore, is unlikely to be regulated by PSA expression. In contrast, the improved ability of Schwann cells to integrate among astrocytes is consistent with a role for PSA in promoting repulsion between strongly adherent cells (Johnson *et al*., 2005). Alternatively, improved mixing between the two cell types may have resulted from accelerated Schwann cell migration rather than decreased Schwann cell–astrocyte adhesion. However, our *in vitro* experiments showed that astrocytes moved into the Schwann cell's domain rather than the opposite, thus refuting the latter argument.

Improved migration leads to enhanced exogenous remyelination

PSA-NCAM expression by STX-SC was transient *in vivo*. The temporal regulation of PSA-NCAM by the grafted Schwann cells was compatible with a direct role for PSA in Schwann cell exit from the graft and their migration into the intermediate zone, events occurring mainly during the first 2 weeks post-transplantation. Furthermore, PSA downregulation, observed at later time points, is a prerequisite for Schwann cell differentiation in myelin forming cells and was also observed in neonate mouse Schwann cells (Lavdas *et al*., 2006; Papastefanaki *et al*., 2007). Although the mechanism regulating PSA expression remains obscure, it might result from post-transcriptional regulation triggered by Schwann cell differentiation. As a consequence, overexpression of PSA in Schwann cells did not impair their myelinating potential. In fact, $P0^{+}/GFP^{+}$ internodes were found in the STX-SC group only, indicating that accelerated recruitment of PSA-NCAM expressing Schwann cells increased their ability to compete for axons with endogenous myelin-forming cells.

Endogenous remyelination in LPC-induced lesions is the fact of endogenous oligodendrocytes and Schwann cells (reviewed in Zujovic *et al*., 2007). While the origin of oligodendrocytes remyelination is clearly identified, the source of remyelinating Schwann cells still needs to be determined. Interestingly, we found similar amounts of total P0 positivity in the lesion, indicating that when Schwann cells were grafted remotely from the lesion, endogenous Schwann cell remyelination compensated for the lack of exogenous Schwann cell remyelination. Moreover, the amount of endogenous CNS remyelination was not affected. These results differ from the spinal trauma model in which Schwann cells engineered to express PSA-NCAM promoted endogenous remyelination by both Schwann cells and oligodendrocytes (Papastefanaki *et al*., 2007). The low potential of exogenous remyelination is in contrast with studies in which adult macaque

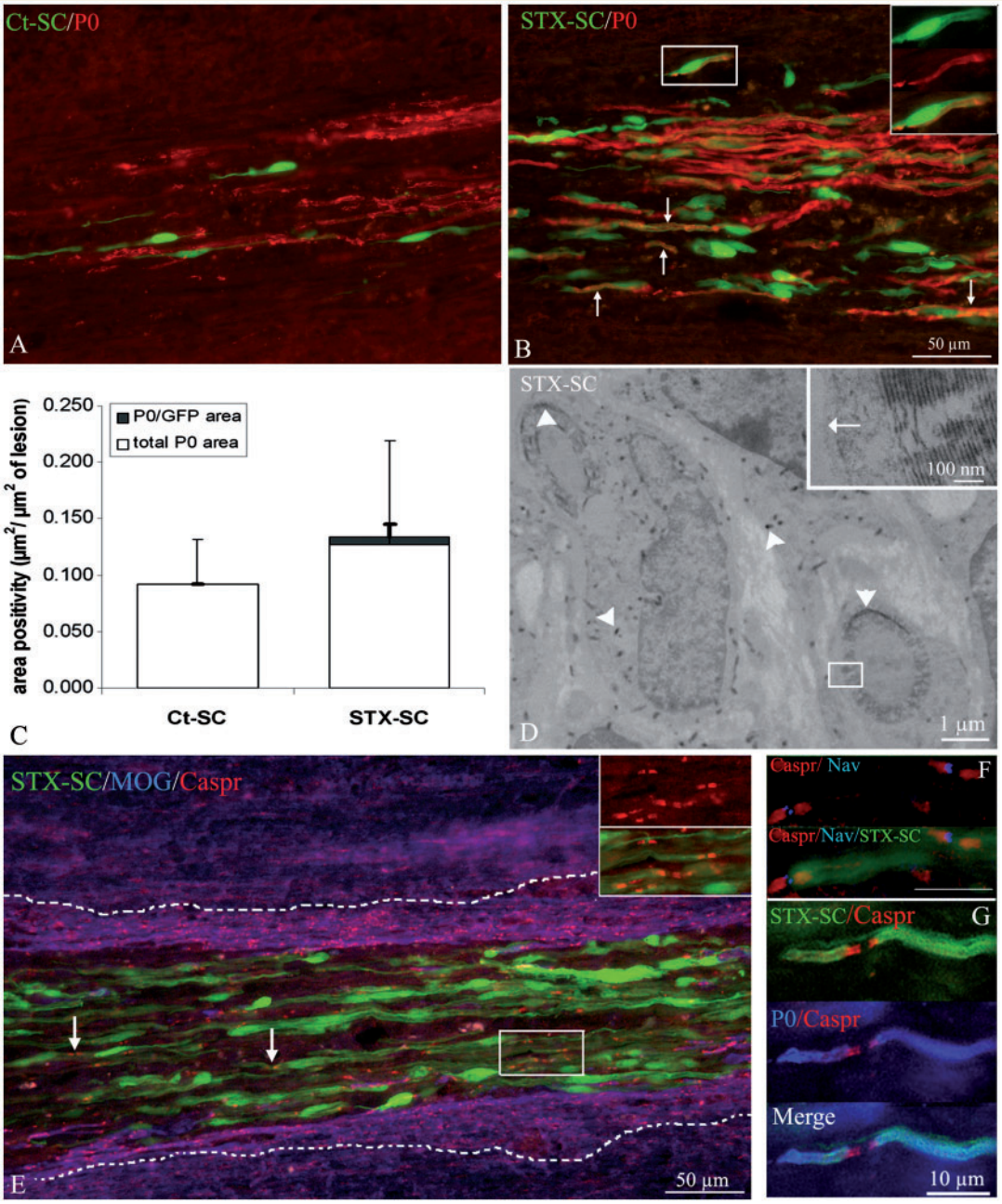

Figure 9 Remyelination potential of Schwann cells grafted into the demyelinated spinal cord. **(A** and **B)** Double detection at the lesion site, of P0 (red) and GFP (green) on horizontal sections of the spinal cords grafted with Ct-SC **(A)** and STX-SC **(B)** 28 d.p.t. While $P0^+$ myelin profiles were observed in both groups, $GFP^+/P0^+$ myelin profiles (arrows, exogenous Schwann cells) were detected in the STX-SC grafted animals only **(B)**. Insert in **B** illustrates a higher magnification of the boxed area. **(C)** Quantification of the total $P0^+$ area indicated no difference in global remyelination by Schwann cells between the control and STX groups. Remyelination by the transplanted Schwann cells ($P0^+/GFP^+$) occurred in the STX-SC group only, the majority of Schwann cell remyelination being performed by the endogenous cells ($P0^+/GFP^-$). At the ultrastructural level, GFP was detected with Bluo-Gal precipitates (**D**, black precipitates). A close up of the boxed area illustrates the presence of a basal lamina (arrow) around the compact myelin. The poor preservation of myelin is due to the stringent immuno-labelling conditions to detect GFP. Immuno-labelling for MOG (blue), Caspr (red) and GFP (green) shows that STX-SC are associated with $Caspr^+$ internodes (red). **(E)** Triple immuno-labelling illustrates STX-SC (green) associated with nodal Na_v (blue) and paranodal Caspr (red) **(F)**. $P0^+$ myelin profiles (blue) produced by STX-SC (green) are associated with $Caspr^+$ paranodes (red) **(G)**.

GFP$^+$ Schwann cells grafted within the lesion of the macaque (Bachelin *et al*., 2005) or nude mouse spinal cord (Girard *et al*., 2005), participated more vigorously to the remyelination process contributing up to 50% of the total peripheral nervous system remyelination. This demonstrates that the amount of competition between endogenous and exogenous Schwann cells is clearly dictated by their respective availability when remyelination onsets. In the context of grafting away from the lesion, cells arrive later and their ability to compete with exogenous Schwann cells drops to zero unless overexpressing PSA-NCAM.

Since PSA-NCAM expression by Schwann cells had no obvious effect on global remyelination of the lesion, functional assays to test the clinical performance of the grafted hosts were not performed. Instead, we questioned the ability of STX-SC-derived myelination to reconstruct normal nodes and paranodes of Ranvier, which are lost as a result of demyelination (Craner *et al*., 2003; Coman *et al*., 2006). We found that grafted adult macaque Schwann cells were able to re-establish the proper pattern of nodal and paranodal proteins with Na_v at the node, flanked by Caspr in the paranodes, a process which correlates with improved neural conduction (Black *et al*., 2006; Sasaki *et al*., 2006).

Conclusion and therapeutic implications

Schwann cell-based therapy has been limited by the poor capacity of Schwann cells to migrate in the CNS. The present study provides evidence that STX-SC are able to migrate through normal CNS by taking a specific path: the dorsal spinal midline. Increased inter-Schwann cell fluidity, Schwann cell–astrocyte mixing and/or Schwann cell–extra-cellular matrix interaction, promoted their efficient migration leading to enhanced recruitment by distant lesions. As a result, only PSA-NCAM overexpressing cells were able to compete with endogenous cells for remyelination and to redirect channel protein organization on healthy axons. Thus, forced PSA expression on Schwann cells may have important therapeutic implications for the treatment of myelin diseases with widespread lesions such as those encountered in multiple sclerosis.

Acknowledgements

We would like to thank Dr Nait-Oumesmar for his critical review of the paper. We are grateful to the Pitié-Salpêtrière Imaging facility for their technical assistance. We thank E. Peles for the generous gift of Caspr antibody (Weizmann Institute of Science, Rehovot, Israël) and M. Carnaud (INSERM U536) for technical advice on ion channel identification.

Funding

Wings for Life, INSERM and AP-HP; Contrat d'interface to AB; fellowship from the Association pour la Recherche sur la Sclérose en Plaques (ARSEP to V.Z.); fellowship from the European Leukodystrophy Foundation (ELA to D.B.).

Supplementary material

Supplementary material is available at *Brain* online.

References

Angata K, Fukuda M. Polysialyltransferases: major players in polysialic acid synthesis on the neural cell adhesion molecule. Biochimie 2003; 85: 195–206.

Avellana-Adalid V, Bachelin C, Lachapelle F, Escriou C, Ratzkin B, Baron-Van Evercooren A. In vitro and in vivo behaviour of NDF-expanded monkey Schwann cells. Eur J Neurosci 1998; 10: 291–300.

Bachelin C, Lachapelle F, Girard C, Moissonnier P, Serguera-Lagache C, Mallet J, et al. Efficient myelin repair in the macaque spinal cord by autologous grafts of Schwann cells. Brain 2005; 128: 540–9.

Baron-Van Evercooren A, Avellana-Adalid V, Ben Younes-Chennoufi A, Gansmuller A, Nait-Oumesmar B, Vignais L. Cell–cell interactions during the migration of myelin-forming cells transplanted in the demyelinated spinal cord. Glia 1996; 16: 147–64.

Baron-Van Evercooren A, Avellana-Adalid V, Lachapelle F, Liblau R. Schwann cell transplantation and myelin repair of the CNS. Mult Scler 1997; 3: 157–61.

Baron-Van Evercooren A, Gansmuller A, Duhamel E, Pascal F, Gumpel M. Repair of a myelin lesion by Schwann cells transplanted in the adult mouse spinal cord. J Neuroimmunol 1992; 40: 235–42.

Black JA, Waxman SG, Smith KJ. Remyelination of dorsal column axons by endogenous Schwann cells restores the normal pattern of Nav1.6 and Kv1.2 at nodes of Ranvier. Brain 2006; 129: 1319–29.

Blakemore WF. Remyelination of CNS axons by Schwann cells transplanted from the sciatic nerve. Nature 1977; 266: 68–9.

Blakemore WF, Franklin RJ. Transplantation options for therapeutic central nervous system remyelination. Cell Transplant 2000; 9: 289–94.

Charneau P, Alizon M, Clavel F. A second origin of DNA plus-strand synthesis is required for optimal human immunodeficiency virus replication. J Virol 1992; 66: 2814–20.

Coman I, Aigrot MS, Seilhean D, Reynolds R, Girault JA, Zalc B, et al. Nodal, paranodal and juxtaparanodal axonal proteins during demyelination and remyelination in multiple sclerosis. Brain 2006; 129: 3186–95.

Craner MJ, Lo AC, Black JA, Waxman SG. Abnormal sodium channel distribution in optic nerve axons in a model of inflammatory demyelination. Brain 2003; 126: 1552–61.

Decker L, Avellana-Adalid V, Nait-Oumesmar B, Durbec P, Baron-Van Evercooren A. Oligodendrocyte precursor migration and differentiation: combined effects of PSA residues, growth factors, and substrates. Mol Cell Neurosci 2000; 16: 422–39.

Duncan ID, Aguayo AJ, Bunge RP, Wood PM. Transplantation of rat Schwann cells grown in tissue culture into the mouse spinal cord. J Neurol Sci 1981; 49: 241–52.

Durbec P, Cremer H. Revisiting the function of PSA-NCAM in the nervous system. Mol Neurobiol 2001; 24: 53–64.

Fairless R, Frame MC, Barnett SC. N-cadherin differentially determines Schwann cell and olfactory ensheathing cell adhesion and migration responses upon contact with astrocytes. Mol Cell Neurosci 2005; 28: 253–63.

Fouad K, Schnell L, Bunge MB, Schwab ME, Liebscher T, Pearse DD. Combining Schwann cell bridges and olfactory-ensheathing glia grafts with chondroitinase promotes locomotor recovery after complete transection of the spinal cord. J Neurosci 2005; 25: 1169–78.

Franklin RJ. Remyelination of the demyelinated CNS: the case for and against transplantation of central, peripheral and olfactory glia. Brain Res Bull 2002; 57: 827–32.

Franklin RJ, Blakemore WF. Requirements for Schwann cell migration within CNS environments: a viewpoint. Int J Dev Neurosci 1993; 11: 641–9.

Girard C, Bemelmans AP, Dufour N, Mallet J, Bachelin C, Nait-Oumesmar B, et al. Grafts of brain-derived neurotrophic factor and neurotrophin 3-transduced primate Schwann cells lead to functional recovery of the demyelinated mouse spinal cord. J Neurosci 2005; 25: 7924–33.

Glaser T, Brose C, Franceschini I, Hamann K, Smorodchenko A, Zipp F, et al. Neural cell adhesion molecule polysialylation enhances the sensitivity of embryonic stem cell-derived neural precursors to migration guidance cues. Stem Cells 2007; 25: 3016–25.

Gout O, Gansmuller A, Baumann N, Gumpel M. Remyelination by transplanted oligodendrocytes of a demyelinated lesion in the spinal cord of the adult shiverer mouse. Neurosci Lett 1988; 87: 195–9.

Hinks GL, Franklin RJ. Delayed changes in growth factor gene expression during slow remyelination in the CNS of aged rats. Mol Cell Neurosci 2000; 16: 542–56.

Honmou O, Felts PA, Waxman SG, Kocsis JD. Restoration of normal conduction properties in demyelinated spinal cord axons in the adult rat by transplantation of exogenous Schwann cells. J Neurosci 1996; 16: 3199–208.

Imaizumi T, Lankford KL, Kocsis JD. Transplantation of olfactory ensheathing cells or Schwann cells restores rapid and secure conduction across the transected spinal cord. Brain Res 2000; 854: 70–8.

Jeffery ND, Blakemore WF. Remyelination of mouse spinal cord axons demyelinated by local injection of lysolecithin. J Neurocytol 1995; 24: 775–81.

Jessen KR, Mirsky R. The origin and development of glial cells in peripheral nerves. Nat Rev Neurosci 2005; 6: 671–82.

Johnson CP, Fujimoto I, Rutishauser U, Leckband DE. Direct evidence that neural cell adhesion molecule (NCAM) polysialylation increases intermembrane repulsion and abrogates adhesion. J Biol Chem 2005; 280: 137–45.

Kohama I, Lankford KL, Preiningerova J, White FA, Vollmer TL, Kocsis JD. Transplantation of cryopreserved adult human Schwann cells enhances axonal conduction in demyelinated spinal cord. J Neurosci 2001; 21: 944–50.

Lakatos A, Barnett SC, Franklin RJ. Olfactory ensheathing cells induce less host astrocyte response and chondroitin sulphate proteoglycan expression than Schwann cells following transplantation into adult CNS white matter. Exp Neurol 2003; 184: 237–46.

Lasiene J, Shupe L, Perlmutter S, Horner P. No evidence for chronic demyelination in spared axons after spinal cord injury in a mouse. J Neurosci 2008; 28: 3887–96.

Lavdas AA, Franceschini I, Dubois-Dalcq M, Matsas R. Schwann cells genetically engineered to express PSA show enhanced migratory potential without impairment of their myelinating ability in vitro. Glia 2006; 53: 868–78.

Levi AD, Bunge RP, Lofgren JA, Meima L, Hefti F, Nikolics K, et al. The influence of heregulins on human Schwann cell proliferation. J Neurosci 1995; 15: 1329–40.

McCarthy KD, de Vellis J. Preparation of separate astroglial and oligodendroglial cell cultures from rat cerebral tissue. J Cell Biol 1980; 85: 890–902.

McTigue DM, Horner PJ, Stokes BT, Gage FH. Neurotrophin-3 and brain-derived neurotrophic factor induce oligodendrocyte proliferation and myelination of regenerating axons in the contused adult rat spinal cord. J Neurosci 1998; 18: 5354–65.

Meintanis S, Thomaidou D, Jessen KR, Mirsky R, Matsas R. The neuron-glia signal beta-neuregulin promotes Schwann cell motility via the MAPK pathway. Glia 2001; 34: 39–51.

Oumesmar BN, Vignais L, Duhamel-Clerin E, Avellana-Adalid V, Rougon G, Baron-Van Evercooren A. Expression of the highly polysialylated neural cell adhesion molecule during postnatal myelination and following chemically induced demyelination of the adult mouse spinal cord. Eur J Neurosci 1995; 7: 480–91.

Papastefanaki F, Chen J, Lavdas AA, Thomaidou D, Schachner M, Matsas R. Grafts of Schwann cells engineered to express PSA-NCAM promote functional recovery after spinal cord injury. Brain 2007; 130: 2159–74.

Pearse DD, Marcillo AE, Oudega M, Lynch MP, Wood PM, Bunge MB. Transplantation of Schwann cells and olfactory ensheathing glia after spinal cord injury: does pretreatment with methylprednisolone and interleukin-10 enhance recovery? J Neurotrauma 2004; 21: 1223–39.

Ranscht B, Clapshaw PA, Price J, Noble M, Seifert W. Development of oligodendrocytes and Schwann cells studied with a monoclonal antibody against galactocerebroside. Proc Natl Acad Sci USA 1982; 79: 2709–13.

Rutishauser U. Polysialic acid in the plasticity of the developing and adult vertebrate nervous system. Nat Rev Neurosci 2008; 9: 26–35.

Rutkowski JL, Kirk CJ, Lerner MA, Tennekoon GI. Purification and expansion of human Schwann cells in vitro. Nat Med 1995; 1: 80–3.

Santos-Silva A, Fairless R, Frame MC, Montague P, Smith GM, Toft A, et al. FGF/heparin differentially regulates Schwann cell and olfactory ensheathing cell interactions with astrocytes: a role in astrocytosis. J Neurosci 2007; 27: 7154–67.

Sasaki M, Black JA, Lankford KL, Tokuno HA, Waxman SG, Kocsis JD. Molecular reconstruction of nodes of Ranvier after remyelination by transplanted olfactory ensheathing cells in the demyelinated spinal cord. J Neurosci 2006; 26: 1803–12.

Sommer I, Schachner M. Monoclonal antibodies (O1 to O4) to oligodendrocyte cell surfaces: an immunocytological study in the central nervous system. Dev Biol 1981; 83: 311–27.

Takami T, Oudega M, Bates ML, Wood PM, Kleitman N, Bunge MB. Schwann cell but not olfactory ensheathing glia transplants improve hindlimb locomotor performance in the moderately contused adult rat thoracic spinal cord. J Neurosci 2002; 22: 6670–81.

Vitry S, Bertrand JY, Cumano A, Dubois-Dalcq M. Primordial hematopoietic stem cells generate microglia but not myelin-forming cells in a neural environment. J Neurosci 2003; 23: 10724–31.

Wilby MJ, Muir EM, Fok-Seang J, Gour BJ, Blaschuk OW, Fawcett JW. N-Cadherin inhibits Schwann cell migration on astrocytes. Mol Cell Neurosci 1999; 14: 66–84.

Yoshimura K, Negishi T, Kaneko A, Sakamoto Y, Kitamura K, Hosokawa T, et al. Monoclonal antibodies specific to the integral membrane protein P0 of bovine peripheral nerve myelin. Neurosci Res 1996; 25: 41–9.

Zennou V, Serguera C, Sarkis C, Colin P, Perret E, Mallet J, et al. The HIV-1 DNA flap stimulates HIV vector-mediated cell transduction in the brain. Nat Biotechnol 2001; 19: 446–50.

Zujovic V, Bachelin C, Baron-Van Evercooren A. Remyelination of the central nervous system: a valuable contribution from the periphery. Neuroscientist 2007; 13: 383–91.